Polymer Chemistry

ROYAL SOCIETY OF CHEMISTRY

PAPER

View Article Online
View Journal

Cite this: DOI: 10.1039/d5py00535c

Synthesis and applications of fused heterocyclic polymers containing naphthoquinone structures†

Chenlei Yu, Xijie Gou, Jingyun Wei, Haoyi Zhang, Di Zhang and Xuediao Cai *

In the field of modern polymer chemistry, developing synthetic strategies to construct fused heterocyclic polymers with novel and unique structures holds significant research value. In this study, we designed and developed a simple and efficient multicomponent polymerization method for constructing fused heterocyclic polymers containing naphthoquinone structures in their main chains. Two synthesized key monomers, 1,4,5,8-anthracenetetrone and 1,1′-dimethyl-5,5′-biindole, were polymerized with aniline in a model polymerization reaction, during which the reaction conditions, such as catalyst, temperature, reaction time, monomer ratio and so on, were systematically screened and optimized. A series of fused heterocyclic polymers containing naphthoquinone structures with high molecular weights (M_n ~ 5000) and relatively high yields (around 70%) were successfully synthesized. The synthesized polymers, attributed to the quinone groups and fused heterocyclic structures presented in the polymer main chain, exhibited excellent thermal stability, narrow electrochemical bandgaps, and desirable fluorescence properties. Leveraging these properties, polymers P2, P5, P13, and P14 were successfully applied in the development of selective fluorescent chemosensors for Fe^{3+} detection. Additionally, a possible polymerization mechanism was proposed in this study, and the binding mechanism between the polymers and metal ions was elucidated. This provides reference and theoretical support for future research in this domain.

Received 30th May 2025,
Accepted 5th July 2025

DOI: 10.1039/d5py00535c

rsc.li/polymers

1. Introduction

With the development of modern technology, the demand for polymer materials with diverse structures and properties has been steadily increasing. Among various polymer structures, fused heterocyclic polymers with unique conjugated structures have garnered widespread attention from researchers due to their excellent thermal stability, easy film-forming ability, high energy storage capacity, and distinctive optoelectronic properties. Nowadays, fused heterocyclic polymers, owing to their outstanding characteristics, have been widely applied in the fields of optoelectronics and sensors, including solar cells, transistors, and chemical sensors.[1–8] In the field of polymer science, the synthesis of fused heterocyclic polymers with diverse structures and excellent properties is gradually becoming a research focus. By incorporating fused heterocyclic structures into the polymer main chain, fused heterocyclic polymers can be successfully prepared, which significantly expands the application scope of organic small molecules.[9–12] The synthesis of functional polymers with novel structures often relies on the development of innovative and efficient synthetic strategies. Multicomponent polymerization (MCP) is one of the conventional approaches in modern polymer chemistry for constructing fused heterocyclic polymers. MCP offers several advantages, such as simple operation, broad substrate applicability, mild reaction conditions, high reaction efficiency, and strong sequence controllability.[13–16] In MCPs, multiple monomers with different functional groups can be simultaneously introduced into the polymerization system, greatly expanding the structural diversity of the synthesized polymers. This approach facilitates the efficient and rapid production of polymers with novel structures and tailored properties.[17,18]

In recent years, naphthoquinone and its derivatives have attracted significant attention from the scientific community due to their excellent properties, making them highly valued molecular structures.[19–25] According to existing literature, current fused heterocyclic polymers exhibit a variety of structures, but studies focusing on the incorporation of naphthoquinone-based structures into those polymers remain limited. If naphthoquinone structures could be introduced into polymer main chains *via* multicomponent polymerization to synthesize naphthoquinone-based fused heterocyclic polymers, it would provide an opportunity for naphthoquinone structures to achieve diverse properties and applications in polymeric form. This approach would also partially address the research gap in modern polymer chemistry regarding

Key Laboratory of Macromolecular Science of Shaanxi Province, School of Chemistry and Chemical Engineering, Shaanxi Normal University, No. 620, West Chang'an Avenue, 710119 Xi'an, P. R. China. E-mail: xdcai@snnu.edu.cn

† Electronic supplementary information (ESI) available. See DOI: https://doi.org/10.1039/d5py00535c

naphthoquinone-based fused heterocyclic polymers. Therefore, developing an efficient and straightforward method for synthesizing fused heterocyclic polymers with naphthoquinone structures in the main chain is of great significance. It is well known that most polymerization reactions often evolve from small-molecule reactions.[26] Therefore, the construction of naphthoquinone-based fused heterocyclic polymers requires corresponding chemical reactions as a foundation. Currently, various studies on the synthesis of naphthoquinone-based fused heterocyclic compounds have been reported. For example, Wang's team proposed in 2009 a reaction using 1,4-naphthoquinone doubly modified with hydroxyl and amino groups as the substrate, with tetrahydrofuran as the solvent, conducted at temperatures ranging from 0 °C to room temperature (Fig. 1A).[27] In 2017, Bayat's team reported a reaction using hydroxyl-monofunctionalized naphthoquinone as the substrate and methanol as the solvent (Fig. 1B).[28] However, these reactions did not gain further attention from researchers due to the complexity and high cost of the raw materials, as well as their relatively low yields. It was not until 2022 that Kumari's team developed a peroxide-free one-pot method to directly synthesize *ortho*-disubstituted naphthoquinones. Conducted under atmospheric conditions, the reaction enabled the synthesis of structurally stable and highly extendable naphthoquinone-based fused heterocyclic compounds with relatively high yields (Fig. 1C).[29] Based on the small-molecule reactions, we hypothesized that modifying the monofunctional monomers in the small-molecule reactions into bifunctional monomers could enable polymerization. Therefore, we designed a novel multicomponent polymerization reaction to synthesize and explore new types of naphthoquinone-based fused heterocyclic polymers with diverse functionalities (Fig. 1D).

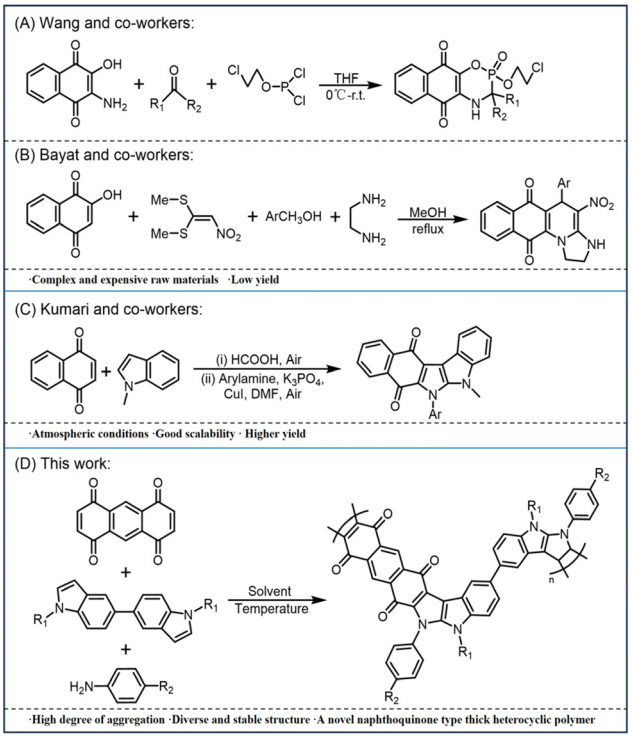

Fig. 1 (A–C) Previously reported methods for constructing naphthoquinone-based fused heterocyclic compounds. (D) The polymerization reaction designed in this study.

2. Results and discussion

Polymerization

To investigate and optimize this polymerization method for the efficient and flexible preparation of naphthoquinone-based fused heterocyclic polymers, a series of corresponding monomers were designed. M1 and M2 were synthesized using existing methods (details of the synthesis steps are provided in the ESI†),[30–33] while the aromatic amine M3 was commercially available. Based on the polymerization method developed in this study (Fig. 1D), we initially performed a preliminary polymerization reaction using readily available 1,4,5,8-anthracenetetrone (M1), 1,1′-dimethyl-5,5′-bi-1*H*-indole (M2a), and aniline (M3a) as monomers, CuI as the catalyst, and formic acid as the solvent. A high-molecular-weight polymer P1 (M_w = 8098 and M_n = 7059) was obtained with a yield of 79.8% (Table 1, entry 1). To achieve higher yields and a better molecular weight distribution, various conditions of this novel multicomponent polymerization reaction were systematically investigated. The optimized parameters included the solvent type, catalyst type, monomer concentration, monomer ratio, reaction atmosphere, reaction temperature, and reaction time. Considering that K_3PO_4 had been added as a base catalyst in the small-molecule reaction literature primarily referenced in this study,[29] we initially attempted several sets of reactions incorporating K_3PO_4 into the polymerization system during the preliminary condition exploration phase (Table S1†). It can be observed that when K_3PO_4 was added to the polymerization system, the yield of polymer progressively decreased as the amount of K_3PO_4 increased. We speculate that the formation of the polymer chain was influenced by the strong alkalinity of K_3PO_4 and led to the low yield. Therefore, in this study, we ultimately chose the reactive conditions without the addition of K_3PO_4 to the reaction system. As shown in Table S2,† a series of common solvents were evaluated. The data in Table S2† indicated that the use of solvents other than formic acid adversely affects the polymerization reaction, resulting in a sharp decrease in yield. This is primarily because formic acid acts as a catalyst in the reaction,[29] whereas other solvents lack this unique catalytic effect, significantly reducing the reaction efficiency. Considering the influence of reaction temperature on the polymerization process, a series of control experiments were conducted at temperatures ranging from 20 °C to 100 °C (Table 1, entries 1–3). The data indicate that lowering the reaction temperature negatively affects the polymerization reaction, and when the temperature is reduced to 20 °C, the polymerization becomes nearly unfeasible. Reaction time also significantly impacts polymerization efficiency and was therefore systematically investigated. Control experiments were conducted

Table 1 Optimization of the polymerization reaction model[a]

Entry	Catalyst/mol%	Solvent/C_M (mol L^{-1})	[M1]/[M2a]/[M3a]	Atmosphere	T. (°C)	Time (h)	Yield[b] (%)	M_n [c]	M_w [c]	PDI[c]
1	CuI	FA	1 : 1 : 1	Air	100	48	79.8	7059	8098	1.15
Screening reaction temperature										
2	CuI	FA	1 : 1 : 1	Air	50	48	49.5	2357	3987	1.69
3	CuI	FA	1 : 1 : 1	Air	20	48	Trace[d]	—	—	—
Screening response time										
4	CuI	FA	1 : 1 : 1	Air	100	24	58.3	4371	5932	1.36
5	CuI	FA	1 : 1 : 1	Air	100	72	82.0	8976	10 742	1.19
Screening atmosphere										
6	CuI	FA	1 : 1 : 1	Air	100	48	25.9	3109	4128	1.33
Screening monomer ratio										
7	CuI	FA	1 : 2 : 1	Air	100	48	72.1	6878	11 165	1.62
8	CuI	FA	2 : 1 : 1	Air	100	48	60.2	5836	7789	1.33
Screening catalyst dosage										
9	CuI (10)	FA	1 : 1 : 1	Air	100	48	71.7	6038	7219	1.20
10	CuI (5)	FA	1 : 1 : 1	Air	100	48	61.9	4856	6146	1.27
11	CuI (30)	FA	1 : 1 : 1	Air	100	48	76.0	5015	8462	1.69
12	CuI (40)	FA	1 : 1 : 1	Air	100	48	77.8	6072	7753	1.28
Screening solvent dosage										
13	CuI	FA (0.05)	1 : 1 : 1	Air	100	48	75.2	4687	6098	1.30
14	CuI	FA (0.2)	1 : 1 : 1	Air	100	48	82.4	7289	8867	1.22
15	CuI	FA (0.3)	1 : 1 : 1	Air	100	48	Gel[e]	—	—	—

[a] Unless otherwise specified, the polymerization reactions were conducted under atmospheric conditions with [M1a] = [M2a] = [M3a] = 0.1 M and [catalyst] = 20 mol%. [b] The yield was calculated after removing insoluble solid impurities *via* filtration, followed by dialysis to remove oligomers with molecular weights lower than 2000. [c] GPC measurements were performed using DMF as the eluent, with polystyrene as the standard reference. The polydispersity index (PDI) of the polymer is defined as PDI = M_w/M_n. [d] Trace indicates that only a very small amount of product was obtained after the reaction, insufficient for yield calculation. [e] Gel refers to gelation during the polymerization process, resulting in insoluble, gel-like solid products.

with reaction times ranging from 24 to 72 hours. As shown in Table 1, reducing the reaction time to 24 hours significantly decreases the reaction efficiency (Table 1, entry 4), while extending the reaction time to 72 hours results in a higher yield (82.0%) and a product with a higher molecular weight (M_w = 10 742 and M_n = 8976) (Table 1, entry 5). However, the polymer product obtained with a reaction time of 72 hours exhibits relatively poor solubility. Due to the complex fused heterocyclic structure of the polymer constructed in this study, excessively high molecular weights often lead to reduced solubility. To ensure the production of a series of products with good solubility in subsequent studies, 48 hours was ultimately selected as the optimal reaction time. The effect of the reaction atmosphere was subsequently explored. As shown in Table 1, entry 6, conducting the reaction in the absence of air leads to a sharp decline in yield. This result partially confirms the catalytic effect of oxygen in the reaction. Next, the monomer ratio was investigated. A series of control experiments with different monomer ratios were conducted to examine the effects of excess M1 or M2 on the polymerization reaction. As shown in the data, an excess of M2a results in polymer products with higher molecular weights, but this is accompanied by a significant decrease in yield and a noticeable broadening of molecular weight distribution (Table 1, entry 7). Conversely, an excess of M1 negatively affects both the yield and the molecular weight of the polymer product (Table 1, entry 8). In summary, an excess of either monomer in this polymerization reaction leads to a decrease in yield and the generation of numerous by-products. Therefore, to ensure reaction efficiency and product structural accuracy, a 1 : 1 : 1 monomer ratio was ultimately selected as the optimal condition. Catalysts often have a significant impact on polymerization reactions. In this study, the type and amount of catalyst were explored. As shown in Table S3,† various catalysts were evaluated. The data indicate that when each type of catalyst is added at 20 mol%, CuI exhibits the best catalytic performance, leading to the highest yield and the most favorable molecular weight. After identifying CuI as the catalyst, its loading was further investigated. In this study, control experiments were conducted with catalyst amounts ranging from 5 mol% to 40 mol%. As shown in Table 1, entries 9–12, when the catalyst amount is 5 mol% or 10 mol%, the molecular weight of the polymer product decreases. However, increasing the catalyst amount to 30 mol% or 40 mol% results in a broadening of the molecular weight distribution (Table 1, entries 11 and 12). Considering the effects of the catalyst on the molecular weight and molecular weight distribution of the product, a catalyst loading of 20 mol% CuI was determined to provide the best catalytic performance. Finally, the effect of monomer concentration on the polymerization reaction was studied. Reducing the monomer concentration to 0.05 M decreased the reaction yield, and the molecular weight of the resulting polymer was relatively low (Table 1, entry 13). Increasing the monomer concentration to 0.2 M further improved the yield, albeit at the expense of a slightly broader molecular weight distribution (Table 1, entry 14). However, further increasing the monomer concentration

to 0.3 M caused gelation of the reaction system, resulting in a large amount of insoluble products (Table 1, entry 15). To ensure the highest possible yield in subsequent studies, the optimal monomer concentration was determined to be 0.2 M, corresponding to the conditions in Table 1, entry 14.

After determining the optimal polymerization conditions, subsequent research aimed to expand the applicability of this polymerization reaction (Scheme 1) by exploring various monomer combinations to synthesize naphthoquinone-based fused heterocyclic polymers with distinct structures and properties. The results are summarized in Table 2. First, R2 was varied while keeping R1 as a methyl group. When a methyl substituent was introduced at the *ortho* position relative to the amino group of M3, the corresponding product was obtained; however, both the yield and molecular weight significantly decreased (Table 2, entry 2). This phenomenon is likely due to the steric hindrance induced by the *ortho*-substituent, which adversely impacts the polymerization process. Since *ortho*-substituted aniline derivatives are relatively rare, subsequent studies focused on aniline derivatives with *para*-substitution on the amino group as M3. Entries 3–5 in Table 2 detail polymerization results using electron-donating substituents on the aromatic amine, while entries 6–10 describe the outcomes when M3 is replaced with aromatic amines substituted with electron-withdrawing groups. The data indicate that the yields of the expansion reactions decreased to some extent across all groups. This decline in yield may be attributed to the steric hindrance effects of the substituents on M3, which interfere with the cyclization reaction during polymerization. Fortunately, the corresponding polymers were successfully obtained in all expansion reactions, demonstrating the versatility and controllability of this system. Encouraged by these results, further studies explored the extension of the R1 group on M2. To enhance the solubility of the resulting polymer, M2b with an ethyl group was introduced by using a previously reported methodology. This monomer was then polymerized with two other types of monomers, resulting in four usable polymers (Table 2, entries 11–14). Based on the data, M2b containing longer side chains also negatively impacted the polymerization process with low yields. These effects may arise

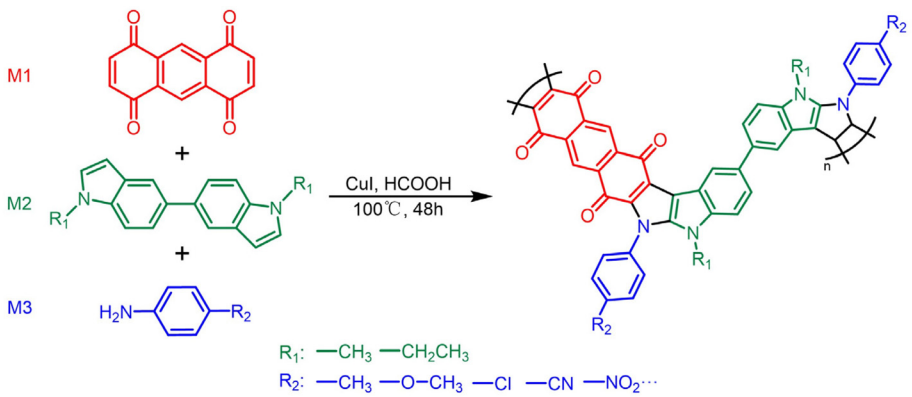

Scheme 1 Schematic representation of the polymerization expansion strategy.

Table 2 Polymerization results of various monomers[a]

Polymers	R_1	R_2	Yield[b] (%)	M_n [c]	M_w [c]	PDI[c]
P1	$-CH_3$	–H	82.4	7289	8867	1.22
P2	$-CH_3$	$-CH_3$ (*ortho*-position)	49.8	4359	5417	1.24
P3	$-CH_3$	$-CH_3$	69.3	7319	8962	1.22
P4	$-CH_3$	$-OCH_3$	74.2	6938	8335	1.20
P5	$-CH_3$	$-OCH_2CH_3$	63.3	6027	7235	1.20
P6	$-CH_3$	$-COCH_3$	70.4	6732	8038	1.19
P7	$-CH_3$	–COOH	66.4	6778	8879	1.31
P8	$-CH_3$	–CN	56.8	5318	6738	1.27
P9	$-CH_3$	–Cl	62.2	6457	7833	1.21
P10	$-CH_3$	$-NO_2$	67.5	6854	7968	1.16
P11	$-CH_2CH_3$	$-NO_2$	59.6	5854	7493	1.28
P12	$-CH_2CH_3$	–CN	61.4	6032	7358	1.22
P13	$-CH_2CH_3$	–H	67.5	6898	8024	1.16
P14	$-CH_2CH_3$	$-CH_3$	66.9	6732	7938	1.18

[a] Unless otherwise noted, polymerization reactions were conducted in formic acid solution at 100 °C for 48 hours under conditions of [1a] = [2a] = 0.2 M and [CuI] = 20 mol%. [b] Yields were calculated after removing insoluble solid impurities *via* filtration followed by dialysis to exclude oligomers with molecular weights below 2000. [c] GPC data were obtained using DMF as the eluent with polystyrene as the standard. PDI represents the polydispersity index of the polymer, defined as PDI = M_w/M_n.

from the longer side chains interfering with monomer stacking behavior and altering the reaction kinetics, thereby hindering effective molecular interactions during polymerization and adversely affecting the overall efficiency of the polymerization reaction.[34]

Structural characterization

After completing the extension reactions for the other 13 groups, a series of structural characterization studies (including ^{1}H NMR, ^{13}C NMR, and IR) were performed on the obtained products to ensure the structural accuracy of the polymerization products. Here, polymer P4 is taken as an example for illustration. In comparison with polymer P4, a model compound was synthesized by reacting 1,4-naphthoquinone, 1-methylindole, and 4-methoxyaniline (details in the ESI†). The ^{1}H NMR and IR spectra of M1, M2a, M3d, the model compound, and P4 are shown in Fig. 2. In the ^{1}H NMR spectra of P4 and the model compound (Fig. 2A), clear resonance peaks corresponding to the hydrogen atoms at position a on M1 (chemical shift at 8.08 ppm), position b on M2a (chemical shift at 3.74 ppm), and position e on M3d (chemical shift at 3.52 ppm) can be observed at similar chemical shifts, with the resonance peaks for positions b and e slightly shifting to higher fields. Additionally, the resonance peaks for positions c (chemical shift at 7.89 ppm) and d (chemical shift at 7.61 ppm) on M2a are not observed in the ^{1}H NMR spectrum of P4. These findings indicate the occurrence of both the model reaction and the polymerization reaction. Furthermore, the IR spectra of P4, its corresponding monomers, and the model compound (Fig. 2B) provide further confirmation of the polymer's structural accuracy. In the IR spectra of the model compound and P4, characteristic peaks can be clearly identified, including the carbonyl peak from M1 (1612 cm^{-1}), the methyl peak from M2a (1516 cm^{-1}), the C–N peak from the tertiary amine in M2a (1262 cm^{-1}), and the methoxy peak from M3d (1122 cm^{-1}). Additionally, the N–H stretching vibration peak at 3300 cm^{-1} induced by the amino group on M3d disappears in both the model compound and P4, strongly confirming that the amino group on M3d successfully participated in the cyclization reaction. Moreover, in the ^{13}C NMR spectrum of P4 (Fig. S53†), the characteristic peaks corresponding to the three monomers can all be found in the polymer's spectrum. In summary, all of these characterization results comprehensively demonstrate the successful synthesis of the target polymer with a well-defined structure. The other 13 types of

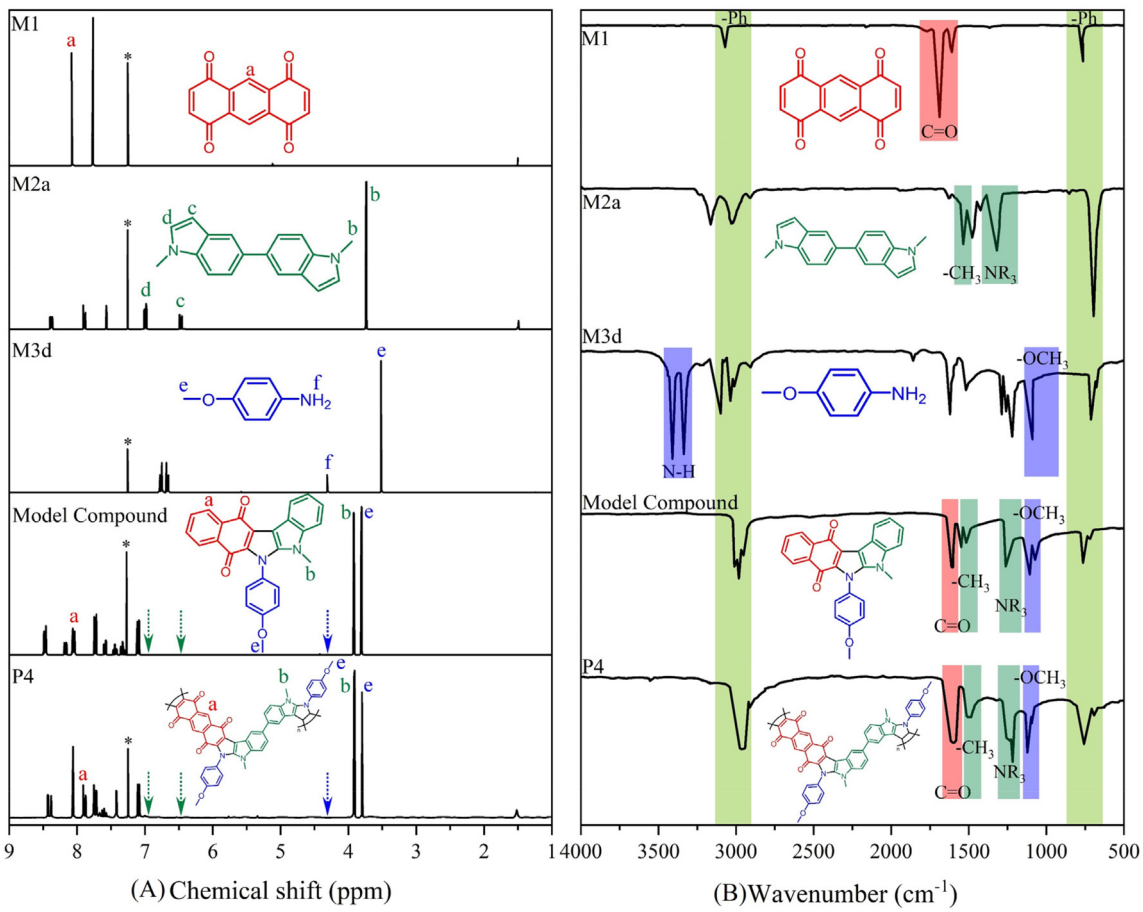

Fig. 2 (A) ^{1}H NMR spectra of M1, M2a, M3d, the model compound, and P4. (B) IR spectra of M1, M2a, M3d, the model compound, and P4.

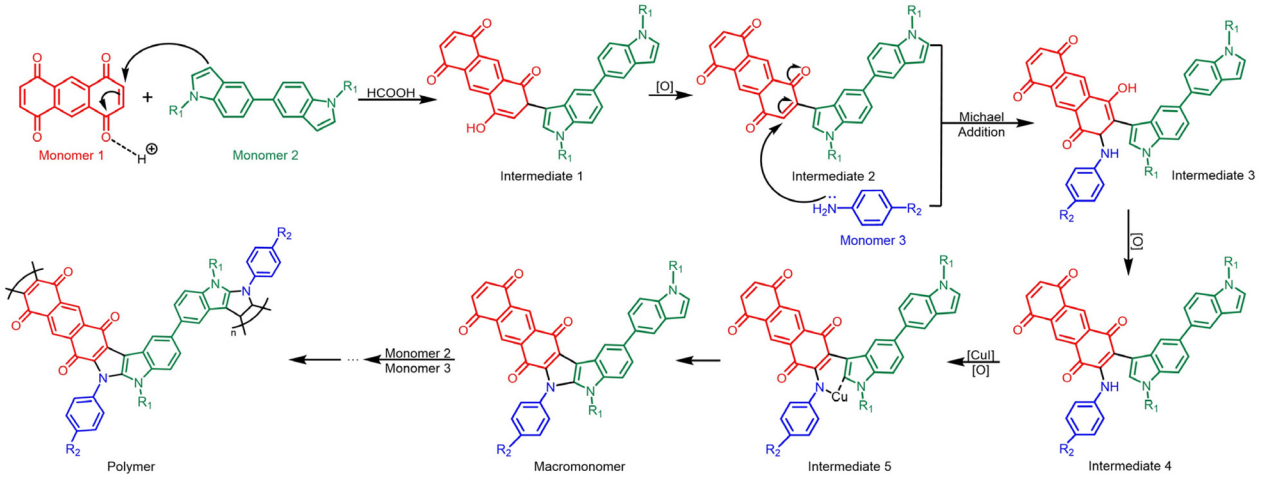

Scheme 2 Proposed polymerization mechanism in this study.

polymers and their corresponding monomers were characterized using the same approach, and the results are provided in the ESI.†

Based on a review of small-molecule reaction mechanisms reported in key references, combined with the polymerization results and structural characterization data obtained in this study, we propose a plausible reaction mechanism for the polymerization process, as illustrated in Scheme 2. Initially, M1 and M2 undergo a nucleophilic addition reaction catalyzed by formic acid, generating intermediate 1. Subsequently, intermediate 1 undergoes an oxidation reaction to yield intermediate 2. The aromatic amine M3 then participates in a Michael addition reaction with intermediate 2, forming intermediate 3. Intermediate 3 is further oxidized to generate intermediate 4, which undergoes intramolecular cyclization catalyzed by the copper catalyst to form a macromolecular monomer. This macromolecular monomer continues cycling through this process, ultimately yielding the desired polymer product.

Thermal performance analysis

It is well understood that good thermal stability is a key requirement for polymers to be successfully applied under high-temperature conditions. This is because polymers are prone to a range of complex physical or chemical changes in high-temperature environments, such as degradation, oxidation, or cross-linking. These changes often lead to a significant decline in performance or even a complete loss of functionality. Therefore, ensuring excellent thermal stability not only enhances the reliability and durability of polymers in high-temperature settings but also broadens their application scope and increases their practical value. In this study, thermogravimetric analysis (TGA) was performed on the polymers, with the results presented in Fig. S86–S88† and the relevant data summarized in Table 3. Owing to the unique conjugated rigid structures of these polymers, they exhibited remarkable thermal stability. Most of the polymers exhibited thermal decomposition temperatures exceeding 200 °C. Furthermore, all polymers demonstrated excellent residual mass performance: at 600 °C, the residual mass fraction of all samples exceeded 60%. Overall, these results confirm that the 14 polymers synthesized in this study possess commendable thermal stability. Notably, polymer P14 exhibited the most outstanding thermal performance, with a thermal decomposition temperature (T_d) of 385 °C and a residual mass fraction of 69.9%. This exceptional performance may be attributed to an ideal balance achieved between the substituents and the side chain lengths in P14. This balance moderately enhances the structural stability of the polymer while avoiding the adverse effects associated with excessively long or short side chains. Such optimization likely improves the interplay between rigidity and flexibility in the polymer backbone, enabling the polymer to resist thermal degradation or structural breakdown more effectively under high-temperature conditions, thereby demonstrating exceptional thermal stability.

Optical performance analysis

The optical properties of the polymers synthesized in this study were characterized, focusing on their ultraviolet (UV) absorption spectra and fluorescence emission spectra. The absorption and emission behaviors of the polymers across different wavelength ranges were comprehensively investigated, with the relevant results presented in Fig. 3 and 4. These data provide critical insights into the optical characteristics of the polymers. As shown in Fig. 3, all polymers exhibit two distinct absorption maxima in their UV absorption spectra. These maxima can be attributed to the benzene ring structures of the polymers, which absorb in the 230–270 nm range, and to the π–π* transitions of the complex conjugated structures of the polymers, which absorb in the 300–350 nm range. By comparing Fig. 3A and B, it is evident that the two absorption peaks of the polymers in Fig. 3A have undergone a noticeable redshift relative to those in Fig. 3B. This phenomenon can be explained by the differences in the substituents: polymers P6–P10 in Fig. 3B contain electron-withdrawing

Table 3 Summary of thermal analysis, photochemical, and electrochemical data for P1–P14

Polymers	R_1	R_2	T_d [a] (°C)	Residual rate[b] (%)	λ_{max}^{UV} (nm)	$E_g^{(opt)}$ [c] (eV)	λ_{max}^{PL} (nm)	HOMO[d] (eV)	LUMO[d] (eV)	$E_g^{(elec)}$ [e] (eV)
P1	$-CH_3$	–H	278	69.3	267/311	3.51	523	−5.86	−3.20	2.66
P2	$-CH_3$	$-CH_3$ (*ortho*-position)	228	68.3	268/310	3.53	527	−5.92	−3.13	2.79
P3	$-CH_3$	$-CH_3$	378	71.2	267/312	3.53	528	−5.87	−3.26	2.61
P4	$-CH_3$	$-OCH_3$	379	69.4	267/311	3.52	530	−6.02	−3.07	2.95
P5	$-CH_3$	$-OCH_2CH_3$	196	74.0	267/314	3.51	532	−6.23	−3.10	3.13
P6	$-CH_3$	$-COCH_3$	188	67.6	248/293	3.77	519	−6.18	−3.11	3.07
P7	$-CH_3$	–COOH	221	72.1	247/290	3.79	518	−6.14	−3.01	3.13
P8	$-CH_3$	–CN	303	75.1	249/293	3.78	516	−5.79	−3.02	2.77
P9	$-CH_3$	–Cl	255	64.9	249/292	3.80	513	−5.82	−3.18	2.64
P10	$-CH_3$	$-NO_2$	239	67.4	248/290	3.78	514	−5.61	−3.08	2.53
P11	$-CH_2CH_3$	$-NO_2$	255	68.2	249/292	3.79	525	−6.14	−3.07	3.07
P12	$-CH_2CH_3$	–CN	280	68.1	249/291	3.80	527	−6.21	−3.05	3.16
P13	$-CH_2CH_3$	–H	292	71.8	268/313	3.52	530	−5.84	−3.16	2.68
P14	$-CH_2CH_3$	$-CH_3$	385	69.9	267/313	3.54	534	−5.83	−3.11	2.72

[a] Thermal decomposition temperature refers to the temperature at which the polymer loses 5% of its mass during thermogravimetric analysis under a nitrogen atmosphere at a heating rate of 20 °C min^{-1}. [b] Residual rate refers to the mass fraction of the polymer remaining when the temperature reaches 600 °C. [c] Photochemical band gap is determined through ultraviolet-visible (UV-Vis) absorption spectroscopy. Based on the absorption edge of the material, the band gap value is estimated using the Tauc plot method. The specific calculation process is provided in the ESI.† [d] $E(HOMO) = -e(E_{ox} + 4.74)$ (eV) and $E(LUMO) = -e(E_{red} + 4.74)$ (eV); the specific values are obtained from cyclic voltammetry curves. [e] Electrochemical band gap $E_g = E(LUMO) - E(HOMO)$ (eV).

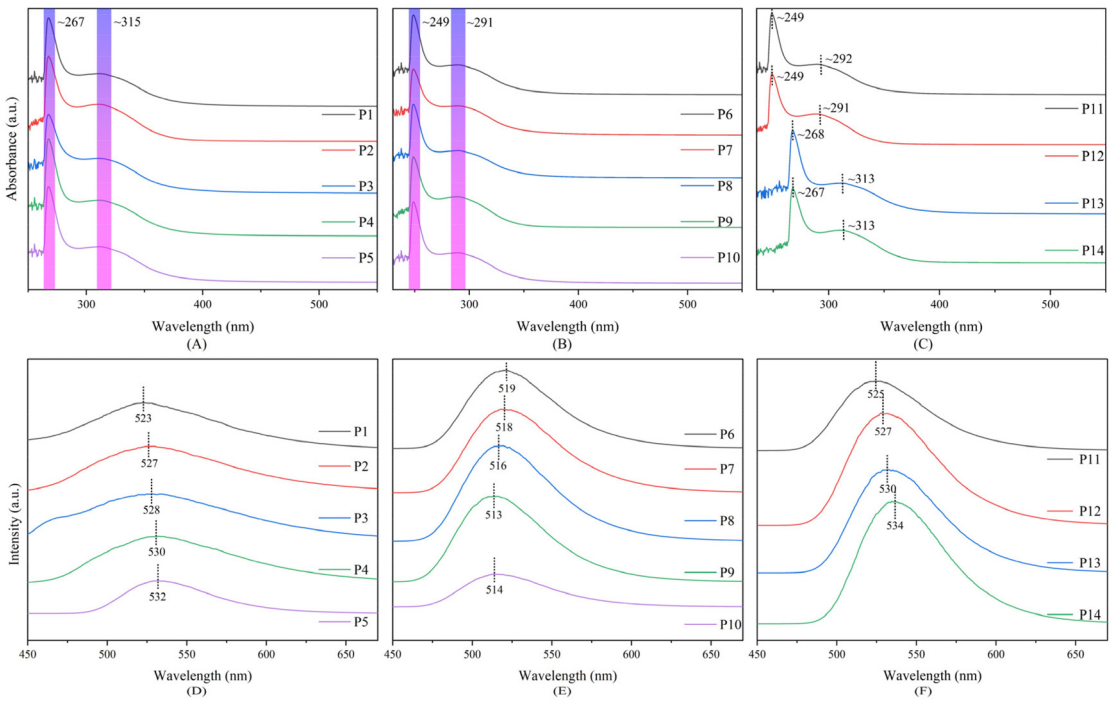

Fig. 3 UV-Vis absorption spectra of different polymers: (A) P1–P5, (B) P6–P10, and (C) P11–P14. Fluorescence emission spectra of different polymers: (D) P1–P5, (E) P6–P10, and (F) P11–P14.

groups, while polymers P1–P5 in Fig. 3A are substituted with electron-donating groups. The introduction of electron-donating groups enhances intramolecular electronic conjugation, effectively lowering the energy level of the polymer's excited state. Additionally, electron-donating groups increase the electron density within the molecule's π-electron system, thereby expanding the molecular π-electron delocalization. This enhancement facilitates a stronger delocalization effect, resulting in a reduction of the excitation energy. Consequently, the maximum absorption peaks in the UV absorption spectra of the polymers shift towards longer wavelengths, exhibiting a redshift. This result is further corroborated in Fig. 3C, where polymers P13 and P14, which contain electron-donating groups, also exhibit a significant redshift compared to polymers P11 and P12. Meanwhile, the UV absorption spectral data were used to calculate the optical bandgaps of the poly-

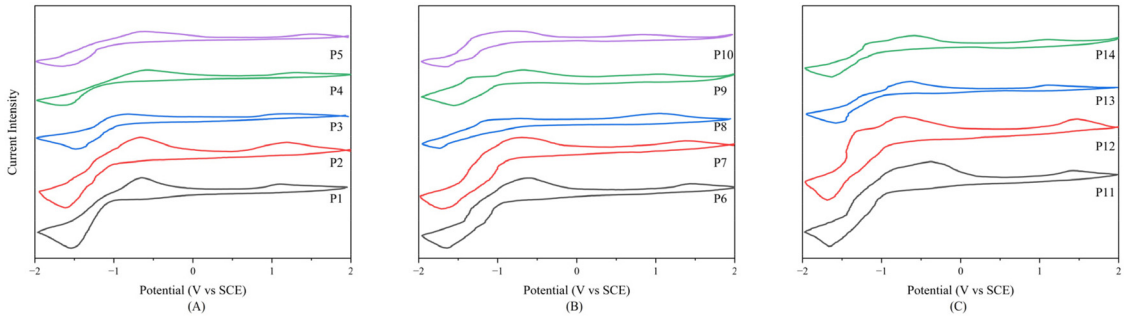

Fig. 4 Cyclic voltammetry (CV) curves of different polymers: (A) P1–P5, (B) P6–P10, and (C) P11–P14 (cyclic voltammetry (CV) testing method: cyclic voltammetry tests were performed on the synthesized fused heterocyclic hyperbranched conjugated polymers using a CHI660E electrochemical workstation. The electrode system of this work-station consisted of a reference electrode (saturated calomel electrode, SCE), a counter electrode (platinum wire), and a working electrode (bare electrode). The specific testing procedure was as follows: a supporting electrolyte solution of 0.1 mol L^{-1} tetrabutylammonium hexafluorophosphate (Bu_4NPF_6) in acetonitrile was prepared. Polymer solutions (5–10 mmol L^{-1} in DMF) were then tested using this electrolyte system).

mers (calculation details are provided in the ESI,† with the results summarized in Table 3). Analyzing the data in Table 3 reveals that the optical bandgaps of polymers P6–P12, which contain electron-withdrawing groups, are significantly larger than those of the groups containing electron-donating substituents. This consistent trend clearly reflects the regulatory effect of different substituents on the optical bandgaps, providing important insights for the design of target photoelectric materials.

Moreover, the influence of different substituents on the polymers is similarly reflected in their fluorescence emission spectra. Specifically, polymers containing electron-donating groups enhance intramolecular electronic conjugation, effectively reducing the energy gap between the excited state and the ground state. This results in a slight shift of the fluorescence emission peak towards longer wavelengths (redshift). Notably, as shown in Fig. 3F, the maximum fluorescence emission wavelengths of polymers P11–P14 are slightly greater than those of the other polymers. This can primarily be attributed to the ethyl side chains present in P11–P14, which effectively reduce intermolecular interactions and increase the degrees of freedom for intramolecular rotation. This increased rotational and vibrational freedom promotes vibrational and rotational transitions within the molecule, thereby reducing the energy gap between the excited and ground states. As a result, the maximum fluorescence emission wavelengths shift further towards longer wavelengths. In summary, these spectral changes clearly illustrate the regulatory effects of different substituents and side chains on the electronic structure of the polymers. These findings provide an important theoretical basis and design strategy for exploring and tuning the optical performance of polymers.

Electrochemical performance analysis

The electrochemical properties of the 14 polymers were systematically analyzed using cyclic voltammetry (CV), and the resulting CV curves are shown in Fig. 4. From these curves, distinct oxidation and reduction peaks can be observed for all polymers, indicating significant reversible redox characteristics during electrochemical analysis. By extracting key data from the CV curves, the corresponding electrochemical bandgaps were calculated, with specific results summarized in Table 3. The data in Table 3 reveal that the electrochemical bandgaps of the polymer groups containing electron-withdrawing groups are slightly larger than those of the groups containing electron-donating groups. The reason behind this observation is that electron-withdrawing groups lower the electron density within the molecule, thereby weakening intramolecular electronic conjugation effects. This results in an increase in the energy level of the lowest unoccupied molecular orbital (LUMO) and a decrease in the energy level of the highest occupied molecular orbital (HOMO), leading to a larger gap between these energy levels (*i.e.*, a larger electrochemical bandgap). In contrast, polymers containing electron-donating groups enhance the electronic conjugation effects, reducing the energy gap and thus leading to smaller electrochemical bandgaps. However, overall, the electrochemical bandgaps of all polymers remain within a relatively small range. Such bandgap characteristics suggest that these polymers can efficiently absorb and utilize a wide range of light energy, thereby demonstrating their potential for the fabrication of high-performance optoelectronic materials.

Construction of metal ion fluorescence sensors

In recent years, fluorescence sensors based on fused heterocyclic polymers have gradually become a research hotspot in the scientific field due to their exceptional sensitivity, stability, and selectivity.[35] At present, sensors constructed based on fused heterocyclic polymers have demonstrated broad application prospects in the field of metal cation detection.[36] In combination with the systematic characterization of polymer properties presented earlier, it can be concluded that the polymers constructed in this study exhibit excellent and easily tunable photochemical and electrochemical properties. These characteristics provide strong support for their practical appli-

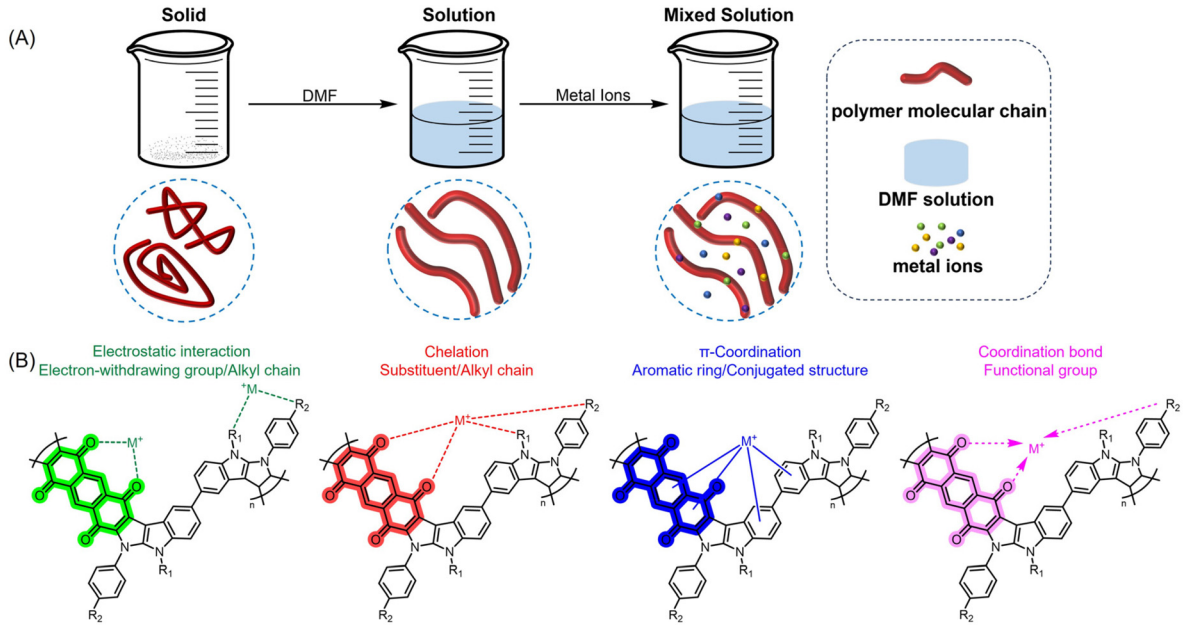

Fig. 5 (A) Schematic illustration of the interaction between polymers and metal ions and (B) the associated binding mechanisms.[37]

cations in metal ion detection and further motivate us to explore their potential value in the field of sensing.

To construct polymer-based fluorescence sensors for metal ions, it is essential to first understand the mechanism of interaction between polymers and metal ions. As depicted in Fig. 5A, polymers in the aggregated state typically exhibit strong intermolecular forces between molecular chains, resulting in twisted and entangled random coil structures. However, when the polymer is dissolved in a good solvent, the intermolecular forces are weakened, allowing the polymer chains to relax and adopt an extended conformation, thereby exhibiting higher solubility and structural flexibility. On this basis, the addition of metal ions to the system significantly enhances the likelihood of interaction between the metal ions and the polymer. This interaction generally leads to noticeable changes in the optical and electrochemical properties of the system, which can serve as an effective basis for the recognition and detection of metal ions. As shown in Fig. 5B, the interaction mechanisms between polymer molecules and metal ions can be primarily categorized into four types: (1) electrostatic interactions between electron-withdrawing groups or alkyl chains and metal ions; (2) chelation effects between substituents or alkyl chains and metal ions; (3) π-coordination effects between the conjugated structures within aromatic rings or polymer chains and metal ions; and (4) coordination bond formation between functional groups and metal ions.[37] These mechanisms not only provide theoretical guidance for the design of polymer-based fluorescence sensors but also enable an in-depth understanding of the structure–property relationship underlying the recognition and detection of metal ions. These interaction mechanisms work synergistically to endow the polymer with excellent metal ion recognition capability. As revealed by the binding mechanisms between metal ions and polymers depicted in Fig. 5B, the naphthoquinone-based fused heterocyclic polymers constructed in this study exhibit significant advantages in metal ion binding. These advantages stem not only from the diverse binding sites provided by the abundant R1 and R2 groups in the polymer molecules but also from the naphthoquinone groups contained within the polymer backbone. The naphthoquinone groups, with their exceptional electron transfer capabilities and π-conjugated characteristics, can efficiently participate in various binding mechanisms between the polymer and metal ions. This multifunctional structural design significantly enhances the binding capability of the naphthoquinone-based fused heterocyclic polymers with metal ions. The synergistic interaction between the polymer and metal ions not only provides higher selectivity and sensitivity during binding but also potentially imparts superior chemical stability and functionality to the polymer.

Encouraged by these findings, we initiated research into the use of naphthoquinone-based fused heterocyclic polymers for constructing metal ion fluorescence sensors. The first step involved performing metal ion selectivity experiments, in which the polymers were mixed with various commonly encountered metal ions and then characterized *via* fluorescence emission spectroscopy. Here, polymer P2 was selected as a representative for detailed discussion (the results for other polymers are provided in the ESI†). As shown in Fig. 6A and B, polymer P2 in solution exhibited a highly specific fluorescence response to Fe^{3+} ions. Upon the addition of Fe^{3+} to the polymer system, the fluorescence intensity rapidly and significantly decreased, showing pronounced fluorescence quenching, with the relative fluorescence intensity dropping to 0.32. This observation clearly indicates that an efficient inter-

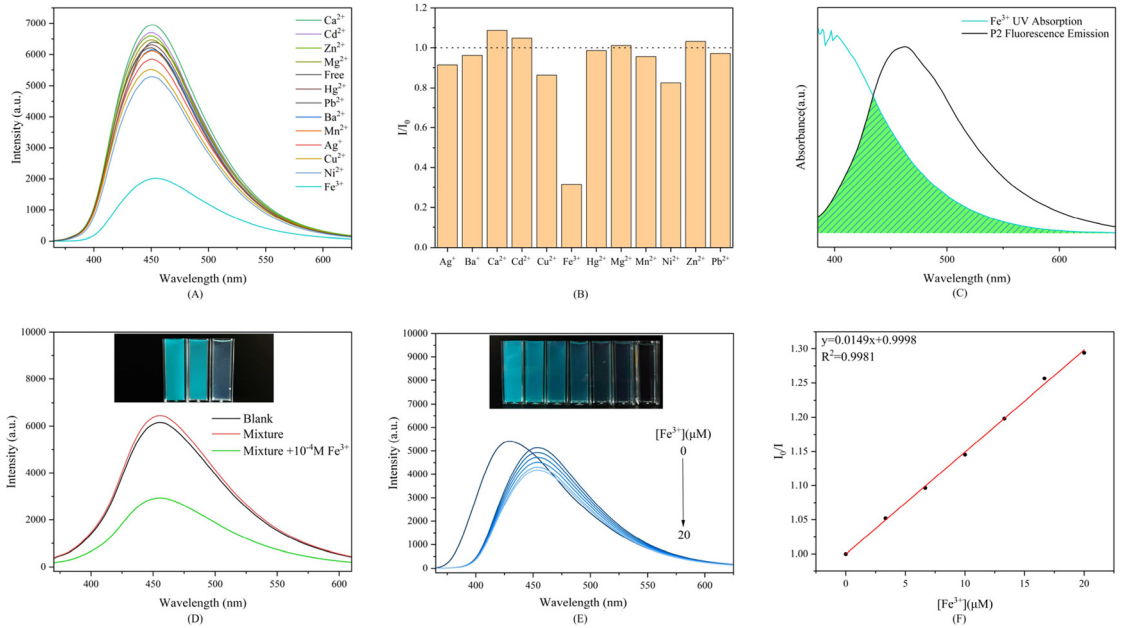

Fig. 6 (A) Fluorescence emission spectra of polymer P2 with the addition of different metal ions. (B) Relative fluorescence intensity values of polymer P2 in the presence of various metal ions. (C) Comparison of the fluorescence emission spectrum of polymer P2 and the UV absorption spectrum of Fe^{3+}. (D) Fluorescence emission spectra of polymer P2 in the presence of mixed metal ions. "Blank" refers to the solution containing only P2, while "Mixture" refers to the solution containing P2 mixed with multiple metal ions (Ag^{+}, Ba^{2+}, Ca^{2+}, Cd^{2+}, Cu^{2+}, Mg^{2+}, Mn^{2+}, Ni^{2+}, Zn^{2+}, and Pb^{2+}). Inset: from left to right are the images taken under UV light for the blank group, the mixed group, and the mixed group with Fe^{3+}. (E) Fluorescence emission spectra of P2 in the presence of varying concentrations of Fe^{3+}. Inset: from left to right are the images taken under UV light as the concentration of Fe^{3+} in the solution gradually increases. (F) Variation curve of the I_0/I value of P2 as a function of Fe^{3+} concentration.

action occurred between polymer P2 and Fe^{3+}, leading to a significant alteration in the fluorescence properties of the polymer. From the results shown in Fig. 6C, it is evident that there is a substantial spectral overlap between the UV absorption spectrum of Fe^{3+} and the fluorescence emission spectrum of P2. It is well known that fluorescence quenching commonly involves non-radiative energy transfer mechanisms between molecules, among which Förster resonance energy transfer (FRET) is the most prevalent. The fundamental condition for FRET is that the energy of a donor in the excited state is transferred to the ground state of an acceptor *via* a non-radiative process, thereby exciting the acceptor. The efficiency of this energy transfer critically depends on the degree of overlap between the fluorescence emission spectrum of the donor and the UV absorption spectrum of the acceptor.[38,39] In other words, if the fluorescence emission wavelength of the excited polymer aligns well with the UV absorption of Fe^{3+} (*i.e.*, strong spectral overlap), the energy transfer efficiency is significantly enhanced, facilitating the rapid transfer of the polymer's excitation energy to the ferric ions. This results in the observed fluorescence quenching of the polymer. This mechanism explains why P2 demonstrates an excellent specific fluorescence response to Fe^{3+}, while also providing theoretical support for the development of Fe^{3+} fluorescence sensors. In realistic environments, sensors are typically exposed to complex mixtures containing multiple ions rather than single metal ion solutions. To simulate such real-world usage conditions, cation competition experiments were conducted in this study to evaluate whether P2 maintains its specific fluorescence response to Fe^{3+} in the presence of multiple coexisting cations. The experimental results, shown in Fig. 6D, clearly indicate that when a mixture of various metal ions is added to the P2 system, no significant change in fluorescence intensity is observed. However, upon the subsequent addition of Fe^{3+} to this mixture, the fluorescence intensity sharply decreases, signifying fluorescence quenching. After confirming the specificity of polymer P2 toward Fe^{3+}, a quantitative study was conducted to evaluate its responsiveness to trace amounts of Fe^{3+} and its detection efficiency at low concentrations. This was achieved by incrementally adding Fe^{3+} solutions with varying concentrations (0, 3.33, 6.67, 10, 13.3, 16.67, and 20 μmol L^{-1}) to the P2 solution. The fluorescence emission spectra of the resulting mixtures at different Fe^{3+} concentrations were then measured, as shown in Fig. 6E. The I_0/I values at the maximum emission peak were plotted against Fe^{3+} concentrations, yielding the curve shown in Fig. 6F. This analysis provides insight into the correlation between the I_0/I value and Fe^{3+} concentration, enabling an accurate assessment of the polymer's detection performance across a broad range of Fe^{3+} concentrations. The results demonstrate that the I_0/I value exhibits a highly linear correlation with Fe^{3+} concentration. This linear relationship can be accurately fitted using the Stern–Volmer equation (eqn (1)) within a small margin of error. In this equation, [Q] represents the quencher (Fe^{3+}) concentration, corresponding to the *x*-axis of the linear equation, and *K* denotes the quenching constant, which is the slope of

Table 4 Detection limits and related data of polymers P2, P5, P13, and P14 for Fe^{3+}

Polymers	Quenching constant, K	δ ($\times 10^{-4}$)	Detection limit, C_L (mol L^{-1})
P2	1.49×10^4	1.92	3.86×10^{-8}
P5	9.37×10^3	2.01	6.45×10^{-8}
P13	7.37×10^3	1.72	7.01×10^{-8}
P14	7.99×10^3	1.58	5.93×10^{-8}

Table 5 Comparison of polymer P2 with other literature-reported Fe^{3+} sensors

Sensor name	Detection limit, C_L (mol L^{-1})	Detection principle
The polymer P2 constructed in this study	3.9×10^{-8}	Fluorescence quenching
Sensor A[44]	1.5×10^{-8}	Fluorescence quenching
PFM[45]	1.2×10^{-7}	Fluorescence quenching
P(AA-*co*-*N*-MA)/PEDOT:PSS hydrogel sensor[46]	9.3×10^{-6}	Conductivity change

the curve.[40,41] Once the quenching constant is obtained, the detection limit (LOD) of polymer P2 for Fe^{3+} can be calculated using an empirical formula (eqn (2)).[42,43] The final calculated detection limit is 3.864×10^{-8} mol L^{-1}, indicating the excellent sensitivity of P2 in detecting trace amounts of Fe^{3+} ions. Compared with other types of Fe^{3+} sensors reported in the literature, the sensor developed in this study exhibits comparable or better detection limits (as shown by the data in Table 5).[44–46] In addition, during practical testing, we discovered that beyond P2, polymers P5, P13, and P14 also exhibited excellent detection capabilities for Fe^{3+}. The detection limits and related data for these polymers have been compiled in Table 4 (corresponding spectra are provided in the ESI†). According to the data in Table 4, all four polymers maintain low detection limits for Fe^{3+}, highlighting their superior detection sensitivity. These findings indicate that the Fe^{3+} fluorescence sensors constructed using P2, P5, P13, and P14 in this study possess significant advantages in sensitivity, making them well-suited for detecting trace amounts of ferric ions in complex environments.

$$I_0/I = 1 + K[Q] \quad (1)$$

$$C_L = 3\delta/k \quad (2)$$

3. Conclusion

In summary, this study successfully developed a novel multicomponent polymerization method for the efficient and direct construction of fused heterocyclic polymers with naphthoquinone structures. This synthetic strategy offers advantages such as high efficiency, excellent scalability, and high atom economy. Through this approach, conjugated fused heterocyclic polymers were obtained while incorporating 1,4-naphthoquinone into the polymer backbone, marking the first successful application of naphthoquinone structures in polymerization reactions. By optimizing and screening various reaction conditions, including the type and amount of catalyst, solvent type, monomer ratio, reaction atmosphere, temperature, and reaction time, the optimal polymerization conditions were obtained. Based on these conditions, the scope of the reactants was expanded, resulting in the successful synthesis of 14 fused heterocyclic polymers with different structures or substituents. Due to the unique naphthoquinone structures in the main chain and the presence of nitrogen-containing fused heterocyclic structures, these polymers exhibit excellent thermal stability (with a maximum T_d of up to 385 °C), narrow electrochemical bandgaps, and outstanding and tunable fluorescence properties. These superior properties endow the polymers with potential applications in the development of fluorescent sensors. In this study, the synthesized products were successfully applied for Fe^{3+} detection, with polymers P2, P5, P13, and P14 demonstrating excellent specificity in their fluorescence responses to Fe^{3+}. The fluorescence intensity of these polymers exhibited a strong linear correlation with Fe^{3+} concentration, with detection limits as low as 3.86×10^{-8} mol L^{-1} in solution. This indicates their potential as fluorescent chemosensors for Fe^{3+}. Moreover, the multicomponent polymerization strategy employed in this study to prepare fused heterocyclic polymers with naphthoquinone structures is expected to provide new inspiration and insights into modern polymer chemistry. It also paves the way for further design, expansion, and applications of naphthoquinone-based polymers across various fields.

Conflicts of interest

There are no conflicts to declare.

Data availability

All data generated or analyzed during this study are included in this published article and its ESI.†

Acknowledgements

This work was supported by the National Key Research Program of China (2016YFA0202403).

References

1 R. Dong, Q. Chen, X. Cai, Q. Zhang and Z. Liu, *Polym. Chem.*, 2020, **11**, 5200–5206, DOI: 10.1039/d0py00680g.
2 C. Luo, Y. Liu, Q. Zhang and X. Cai, *RSC Adv.*, 2017, **7**, 12269–12276, DOI: 10.1039/C7RA00540G.

3 L. Xu, T. Zhou, M. Liao, R. Hu and B. Z. Tang, *ACS Macro Lett.*, 2019, **8**, 101–106, DOI: **10.1021/acsmacrolett.8b00884**.
4 M. Saleh, M. Baumgarten, A. Mavrinskiy, T. Schäfer and K. Müllen, *Macromolecules*, 2010, **43**, 137–143, DOI: **10.1021/ma901912t**.
5 J. Sun, J. Yang, C. Zhang, H. Wang, J. Li, S. Su, H. Xu, T. Zhang, Y. Wu, W. Wong and B. Xu, *New J. Chem.*, 2015, **39**, 5180–5188, DOI: **10.1039/c5nj00289c**.
6 J. Oriou, F. Ng, G. Hadziioannou, G. Garbay, M. Bousquet, L. Vignau, E. Cloutet and C. Brochon, *Polym. Chem.*, 2014, **5**, 7100–7108, DOI: **10.1039/c4py00896k**.
7 Y. He, G. Fu, W. Li, B. Wang, T. Miao, M. Tan, W. Feng and X. Lü, *J. Lumin.*, 2020, **218**, 116847, DOI: **10.1016/j.jlumin.2019.116847**.
8 Y. Zhang, J. W. Y. Lam and B. Z. Tang, *Polym. Chem.*, 2016, **7**, 330–338, DOI: **10.1039/c5py01466b**.
9 S. Lee, S. Chien, J. Chen, S. Wang, L. Wang, B. Lai and C. Wang, *Org. Electron.*, 2019, **66**, 136–147, DOI: **10.1016/j.orgel.2018.12.027**.
10 E. S. Alsolami, H. S. Alorfi, K. A. Alamry and M. A. Hussein, *RSC Adv.*, 2024, **14**, 1757–1781, DOI: **10.1039/d3ra07278a**.
11 D. Fan, D. Wang, T. Han and B. Z. Tang, *ACS Appl. Polym. Mater.*, 2022, **4**, 3120–3130, DOI: **10.1021/acsapm.1c01476**.
12 J. M. Marin-Beloqui, S. Gómez, H. I. Gonev, M. Comí, M. Al-Hashimi and T. M. Clarke, *Chem. Sci.*, 2023, **14**, 812–821, DOI: **10.1039/D2SC06271B**.
13 C. Wang, B. Yu, W. Li, W. Zou, H. Cong and Y. Shen, *Mater. Today Chem.*, 2022, **25**, 100948, DOI: **10.1016/j.mtchem.2022.100948**.
14 Z. Zhang, Z. Tan, C. Hong, D. Wu and Y. You, *Polym. Chem.*, 2016, **7**, 1468–1474, DOI: **10.1039/C5PY01758K**.
15 D. K. Giannopoulos, L. P. Zorba, C. Zisis, M. Pitsikalis and G. C. Vougioukalakis, *Eur. Polym. J.*, 2023, **191**, 112056, DOI: **10.1016/j.eurpolymj.2023.112056**.
16 L. V. Kayser, E. M. Hartigan and B. A. Arndtsen, *ACS Sustainable Chem. Eng.*, 2016, **4**, 6263–6267, DOI: **10.1021/acssuschemeng.6b02302**.
17 M. A. R. Meier, R. Hu and B. Z. Tang, *Macromol. Rapid Commun.*, 2021, **42**, 2100104, DOI: **10.1002/marc.202100104**.
18 D. Liu, H. Zhang, L. Zhang, J. Wang, Z. Chang and H. Cong, *Polym. Chem.*, 2024, **15**, 2408–2415, DOI: **10.1039/D3PY01406A**.
19 M. M. Rahman, M. R. Islam, S. Akash, S. Shohag, L. Ahmed, F. A. Supti, A. Rauf, A. S. M. Aljohani, W. Al Abdulmonem, A. A. Khalil, R. Sharma and M. Thiruvengadam, *Chem.-Biol. Interact.*, 2022, **368**, 110198, DOI: **10.1016/j.cbi.2022.110198**.
20 T. Nakajima, H. Tateno, Y. Miseki, T. Tsuchiya and K. Sayama, *ACS Appl. Mater. Interfaces*, 2021, **13**, 57132–57141, DOI: **10.1021/acsami.1c16777**.
21 J. Miao, X. Dong, Y. Xu, Z. Zhai, L. Zhang, B. Ren and Z. Liu, *Org. Electron.*, 2019, **73**, 304–310, DOI: **10.1016/j.orgel.2019.06.025**.
22 C. Sayil, N. G. Deniz and A. Cinarli, *Prog. Org. Coat.*, 2016, **98**, 39–42, DOI: **10.1016/j.porgcoat.2016.04.017**.
23 C. E. Pereyra, R. F. Dantas, S. B. Ferreira, L. P. Gomes and F. P. Silva-Jr, *Cancer Cell Int.*, 2019, **19**, 207, DOI: **10.1186/s12935-019-0925-8**.
24 N. V. Aseeva, N. V. Danilenko, E. V. Plotnikov, E. I. Korotkova, O. I. Lipskikh, A. N. Solomonenko, A. V. Erkovich, D. D. Eskova and A. I. Khlebnikov, *Int. J. Mol. Sci.*, 2024, **25**, 12245, DOI: **10.3390/ijms252212245**.
25 P. Ravichandiran and S. Vasanthkumar, *J. Taibah Univ. Sci.*, 2015, **9**, 538–547, DOI: **10.1016/j.jtusci.2014.12.003**.
26 A. L. Mayhugh, P. Yadav and C. K. Luscombe, *J. Am. Chem. Soc.*, 2022, **144**, 6123–6135, DOI: **10.1021/jacs.1c12455**.
27 B. Wang, Z. Miao and R. Chen, *Phosphorus, Sulfur Silicon Relat. Elem.*, 2009, **184**, 2739–2748, DOI: **10.1080/10426500903095564**.
28 M. Bayat and S. Nasri, *Tetrahedron Lett.*, 2017, **58**, 3107–3111, DOI: **10.1016/j.tetlet.2017.06.076**.
29 S. P. Kumari, S. P. Anthony and S. S. Ganesan, *New J. Chem.*, 2022, **46**, 16874–16879, DOI: **10.1039/D2NJ02024F**.
30 T. Navale and R. Rathore, *Synthesis*, 2012, **5**, 805–809, DOI: **10.1055/s-0031-1289695**.
31 F. Gloecklhofer, B. Stoeger and J. Froehlich, *Synth. Commun.*, 2018, **48**, 2358–2365, DOI: **10.1080/00397911.2018.1483027**.
32 B. S. Zhang, Y. H. Yang, F. Wang, X. Y. Gou, X. C. Wang, Y. M. Liang, Y. Li and Z. J. Quan, *Chin. J. Chem.*, 2021, **39**, 1573–1579, DOI: **10.1002/cjoc.202100034**.
33 S. Zhang, Y. Han, J. He and Y. Zhang, *Polym. Chem.*, 2023, **14**, 492–499, DOI: **10.1039/D2PY01470J**.
34 Z. Qian, S. Luo, T. Qu, L. A. Galuska, S. Zhang, Z. Cao, S. Dhakal, Y. He, K. Hong, D. Zhou and X. Gu, *J. Mater. Res.*, 2021, **36**, 191–202, DOI: **10.1557/s43578-020-00062-9**.
35 T. Wang, N. Zhang, W. Bai and Y. Bao, *Polym. Chem.*, 2020, **11**, 3095–3114, DOI: **10.1039/d0py00336k**.
36 D. Fan, D. Wang, J. Zhang, X. Fu, X. Yan, D. Wang, A. Qin, T. Han and B. Z. Tang, *J. Am. Chem. Soc.*, 2024, **146**, 17270–17284, DOI: **10.1021/jacs.4c03889**.
37 S. Sabaghi, N. Alipoormazandarani, W. Gao and P. Fatehi, *J. Hazard. Mater.*, 2021, **417**, 125970, DOI: **10.1016/j.jhazmat.2021.125970**.
38 W. Zhang, W. Li, Y. Song, Q. Xu and H. Xu, *Biosens. Bioelectron.*, 2024, **255**, 116244, DOI: **10.1016/j.bios.2024.116244**.
39 L. Li, X. Wang, P. Zhu, H. Li, F. Wang and J. Wu, *Nano Energy*, 2020, **70**, 104476, DOI: **10.1016/j.nanoen.2020.104476**.
40 R. N. Motz, A. C. Sun, D. Lehnherr and S. Ruccolo, *ACS Org. Inorg. Au*, 2023, **3**, 266–273, DOI: **10.1021/acsorginorgau.3c00019**.
41 M. H. Gehlen, *J. Photochem. Photobiol., C*, 2020, **42**, 100338, DOI: **10.1016/j.jphotochemrev.2019.100338**.
42 J. Liu, Y. Zhong, P. Lu, Y. Hong, J. W. Y. Lam, M. Faisal, Y. Yu, K. S. Wong and B. Z. Tang, *Polym. Chem.*, 2010, **1**, 426–429, DOI: **10.1039/C0PY00046A**.
43 J. Wang, D. Wang, E. K. Miller, D. Moses, G. C. Bazan and A. J. Heeger, *Macromolecules*, 2000, **33**, 5153–5158, DOI: **10.1021/ma000081j**.
44 S. Kanan, A. Shabnam, A. A. Mohamed and I. A. Abu-Yousef, *Chemosensors*, 2023, **11**, 308, DOI: **10.3390/chemosensors11050308**.

45 P. Sharma, S. Bhogal, I. Mohiuddin, M. Yusuf and A. K. Malik, *J. Fluoresc.*, 2022, **32**, 2319–2331, DOI: **10.1007/s10895-022-03024-y**.

46 H. Chen, X. Zhan, Z. Hong, W. Ni, C. Zhu, Y. Leng, C. Chen, R. Guo, N. Ma and F. Tsai, *Langmuir*, 2024, **40**, 26714–26722, DOI: **10.1021/acs.langmuir.4c03872**.